Available online at www.sciencedirect.com
ScienceDirect
Surface Science 600 (2006) 5004–5010
SURFACE SCIENCE
www.elsevier.com/locate/susc

# Morphology and defect structure of the $CeO_2$(1 1 1) films grown on Ru(0 0 0 1) as studied by scanning tunneling microscopy

J.-L. Lu [a,b], H.-J. Gao [b], S. Shaikhutdinov [a,*], H.-J. Freund [a]

[a] *Fritz-Haber-Institut der Max-Planck-Gesellschaft, Faradayweg 4-6, 14195 Berlin, Germany*
[b] *Beijing National Laboratory for Condensed Matter Physics, Institute of Physics, Chinese Academy of Sciences, P.O. Box 603, Beijing 100080, China*

Received 19 July 2006; accepted for publication 21 August 2006
Available online 8 September 2006

**Abstract**

The morphology of ceria films grown on a Ru(0 0 0 1) substrate was studied by scanning tunneling microscopy in combination with low-energy electron diffraction and Auger electron spectroscopy. The preparation conditions were determined for the growth of nm-thick, well-ordered $CeO_2$(1 1 1) films covering the entire surface. The recipe has been adopted from the one suggested by Mullins et al. [D.R. Mullins, P.V. Radulovic, S.H. Overbury, Surf. Sci. 429 (1999) 186] and modified in that significantly higher oxidation temperatures are required to form atomically flat terraces, up to 500 Å in width, with a low density of the point defects assigned to oxygen vacancies. The terraces often consist of several rotational domains. A circular shape of terraces suggest a large variety of undercoordinated sites at the step edges which preferentially nucleate gold particles deposited onto these films. The results show that reactivity studies over ceria and metal/ceria surfaces should be complemented with STM studies, which provide direct information on the film morphology and surface defects, which are usually considered as active sites for catalysis over ceria.


*Keywords:* Ceria; Thin films; Defects; Scanning tunneling microscopy

## 1. Introduction

Cerium dioxide ($CeO_2$) is a well-known oxide material owing to its superior oxygen storage-and-release properties, which provide a basis for its use in many catalytic applications [1–3]. Ceria belongs to the group of so called reducible oxides where metal cations can change the oxidation state depending on ambient conditions. When supported on reducible oxides (e.g. titania, iron oxides, etc.), noble metal particles may form interfaces very different from those formed on non-reducible oxides (alumina, silica) (for example, see [4–6]). Recently, ceria has received much attention as a support for gold catalysts in low temperature CO oxidation and water gas shift reactions [7–10]. The nature of the active species in Au catalysts (ionic vs. metallic) is a matter of ongoing debates (see reviews [11,12]). Note only, that for small metal particles and clusters, the interaction with point defects such as neutral or charged oxygen vacancies becomes very important as shown, for example, for Au and Pd clusters on MgO(1 0 0) [13–16]. In this respect, removal of neutral oxygen from the ceria surface is thought to lead to electron localization and, as a result, to a different chemistry [1]. Therefore, the knowledge of defect structure of the ceria surface is inevitable towards a detailed understanding of reactivity of the ceria surfaces and ceria supported metal nanoparticles.

Several research groups are carrying out "surface science" studies using ceria single crystals [18–22]. Since ceria is a wide band gap (~6 eV) insulator, one has to overcome sample charging problems, which are usually circumvented by annealing at elevated temperatures (up to 1200 K) leading to a partial reduction of the ceria. These problems are

* Corresponding author. Tel.: +49 30 8413 4114; fax: +49 30 8413 4105.
*E-mail address:* shaikhutdinov@fhi-berlin.mpg.de (S. Shaikhutdinov).

0039-6028/$ - see front matter © 2006 Elsevier B.V. All rights reserved.
doi:10.1016/j.susc.2006.08.023

less critical for thin films grown on metal single crystal substrates, which provide a good electric and thermal conductivity while employing surface sensitive analytical tools. In addition, oxygen diffusion in the thin films can be easily controlled as opposed to the bulk crystal samples.

To date, crystalline ceria films were grown on different metal substrates such as Pd(1 1 1) [23], Pt(1 1 1) [24–27], Rh(1 1 1) [28,29], Cu(1 1 1) [30], Re(0 0 0 1) [31], Ni(1 1 1) [32] and Ru(0 0 0 1) [32–35]. The films were prepared by physical vapor deposition of Ce in an oxygen environment or in vacuum followed by oxidation at elevated temperatures. The choice of the substrate to a lesser extent is driven by the lattice mismatch since the lattice constants of (1 1 1) metal surfaces (2.7–2.9 Å) are much smaller than that of the close packed surfaces of $CeO_2$ and $Ce_2O_3$ (3.89 and 3.82 Å, respectively). More important is a thermal stability of the films because a high temperature annealing is typically required for preparing extended well-ordered films. The ceria films grown on Ru(0 0 0 1) seem to show the best characteristics: the surface does not loose oxygen at ~1000 K, and there is no evidence for cerium alloying with Ru [32]. These films were extensively studied by Mullins and co-workers using low-energy electron diffraction (LEED), Auger electron spectroscopy (AES), ion scattering spectroscopy and photoelectron spectroscopy [32–35]. However, the morphology and defect structure of these films have not been investigated.

In general, there is a lack of morphological and structural studies of ceria surfaces using scanning probe microscopies (STM and AFM). Nörenberg and Briggs [17,18] and very recently Esch et al. [21] reported on STM studies of the (1 1 1) surface of $CeO_2$ single crystals. Iwasawa and co-workers additionally employed non-contact AFM [20]. Basically, the STM and AFM images showed a hexagonal lattice of protrusions assigned to the outmost close-packed O-layer of $CeO_2$(1 1 1). The visible defects were attributed to the oxygen vacancies created upon vacuum annealing at high temperatures. These vacancies may agglomerate and form dimers and other linear defects as well as triangular trimers. Based on DFT calculations, Esch et al. have suggested the formation of sub-surface oxygen vacancies in order to explain the STM images observed [21]. Note, that these surfaces were produced by vacuum annealing of ceria single crystals at high temperatures, which partially reduces the surface.

Regarding thin ceria films, to the best of our knowledge, Berner and Schierbaum were the first who presented STM images of ceria formed upon oxidation of Ce/Pt(1 1 1) alloy [26]. Netzer and co-workers have recently reported a systematic STM study of ultra-thin ceria films formed on Rh(1 1 1) [28,29]. The authors mainly focused on the initial stages of the film growth. Formation of well-shaped $CeO_2$(1 1 1) islands of ca. 15–20 nm in lateral dimensions was observed upon annealing at ~970 K. Thicker films basically showed agglomeration of the small crystallites, which were difficult to study with a high resolution [28].

For the reactivity studies over oxide films and supported metal particles, it is important to prepare films free of pits, which would expose the metal substrate and possibly determine the observed chemical reactivity. For the case of ceria, this seems to be fulfilled only for the relatively "thick" films due to a large (~40%) mismatch between the ceria and the substrate, which impedes oxide wetting. For example, Wilson et al., using CO adsorption, have observed that about 20% of the Pt(1 1 1) surface are exposed on the films of three monolayers (ML) in average thickness [36]. It is obvious that, for the thick films, the adsorption properties will not be affected by the metal substrate, which still provides a good electric and thermal conductivity of the system. Therefore, in this work, we focus on STM studies of nm-thick ceria films grown on Ru(0 0 0 1), aimed at a better understanding of the morphology and defect structure of the ceria films. This knowledge is to be further used for studying chemical reactivity of pure ceria and ceria supported systems.

## 2. Experimental

The experiments were performed in an ultra-high vacuum (UHV) chamber (base pressure $2 \times 10^{-10}$ mbar) equipped with a STM (Omicron), Auger electron spectroscopy (AES), low energy electron diffraction (LEED) (Specs) and standard facilities for surface cleaning. The Ru(0 0 0 1) single crystal (10 mm diameter and 2 mm thick) was supplied by Mateck. The crystal was clamped to a Mo holder and heated from the backside of the crystal using electron bombardment from a W filament. The temperature was controlled using a type K thermocouple spot-welded to the edge of the crystal and a feedback system (Schlichting Phys. Instrum). The clean surface was prepared using cycles of $Ar^+$ sputtering followed by annealing in UHV to 1300 K. The surface exhibited a sharp $(1 \times 1)$ LEED pattern, and the impurity level was below the detection limit of AES.

Cerium was evaporated from a tungsten crucible heated using ceramic protected W wires wrapped around the crucible. The amounts of Ce is given in monolayers (ML) of $CeO_2$(1 1 1) formed on the Ru surface. At thermal equilibrium reached by slow heating of the crucible to ca. 1500 K, the Ce flux could be controlled either by the current passing through the heating W wire and/or with a thermocouple spot-welded to the crucible. The deposition rates used in this study were in the range of 0.1–0.3 ML/min as calibrated by STM and AES on the clean Ru substrate. Different preparations were tested as discussed below. In order to prevent a partial reduction of ceria films, high temperature annealing was always performed in oxygen, which was pumped out after sample cooled down to 400 K.

The STM images presented in the paper were obtained at room temperature using Pt–Ir tips (L.O.T. Oriel GmbH) at sample bias 2–4 V and tunneling current ~0.1 nA.

## 3. Results and discussion

Following the preparation recipe reported by Mullins et al. [32], the $CeO_2(1\,1\,1)$ films on the Ru(0 0 0 1) crystal can be grown by Ce deposition at ca. 700 K in an oxygen atmosphere. Fig. 1a presents a typical large-scale STM image of the ceria films grown in $1\times10^{-7}$ mbar of $O_2$ at 700 K at sub-monolayer coverage, showing that ceria preferentially nucleates at the steps. The area between the ceria patches is assigned to the reconstructed Ru(0 0 0 1)-$p(2\times2)$O surface since the LEED pattern from this sample showed a superposition of sharp $p(2\times2)$ spots, also observed on the Ce-free samples under the same conditions, and weak $p(1.4\times1.4)$ spots characteristic for ceria. The relative position of the ceria and Ru diffraction spots indicates the alignment of the crystallographic directions of the ceria phase with the principal azimuth directions of Ru(0 0 0 1) as previously reported [32]. The shape and peak position of the $N_5N_{67}O_{45}$ lines in the AES spectra (not shown here) are consistent with those reported in the literature for Ce in $CeO_2$ [37].

The apparent height of the ceria islands with respect to the O/Ru surface is about 5 Å, which, following Eck et al. [28], can be assigned to a bilayer of fluorite type $CeO_2(1\,1\,1)$ with a distance of 3.1 Å between equivalent layers. However, the ceria surface is not atomically flat, on average. There are many particle-like features present on the surface, which must be attributed to ceria clusters since AES spectra revealed no other elements beyond Ru, O and Ce. Further annealing of this sample in $4\times10^{-7}$ mbar of $O_2$ at 900 K (see Fig. 1b) results in larger bilayer islands and small particles, which is characteristic for sintering, proceeding via Ostwald ripening mechanism, where large particles grow at the expense of smaller ones. The large ceria islands exhibit a smooth surface. In addition, the $p(1.4\times1.4)$ diffraction spots of ceria become sharper, indicating a better ordering upon post-oxidation. In line with this observation, increasing the Ce deposition temperature to 790 K promoted film ordering. The film prepared to the same Ce coverage exposes larger islands as compared to deposition at 700 K (see Fig. 1c). Interestingly, these islands exhibited a hexagonal Moire structure with a periodicity ~19 Å (as shown in Fig. 1d), which in a first approximation could be explained by coincidence of seven unit cells length of Ru(0 0 0 1) ($\mathbf{a}_{Ru} = 2.71$ Å) and five unit cells length of $CeO_2(1\,1\,1)$ ($\mathbf{a}_{111} = 3.89$ Å). (Note, that the Moire structure was also reported on ceria bilayer islands formed on Rh(1 1 1) ($\mathbf{a}_{Rh} = 2.69$ Å) [29].) Two domains im-

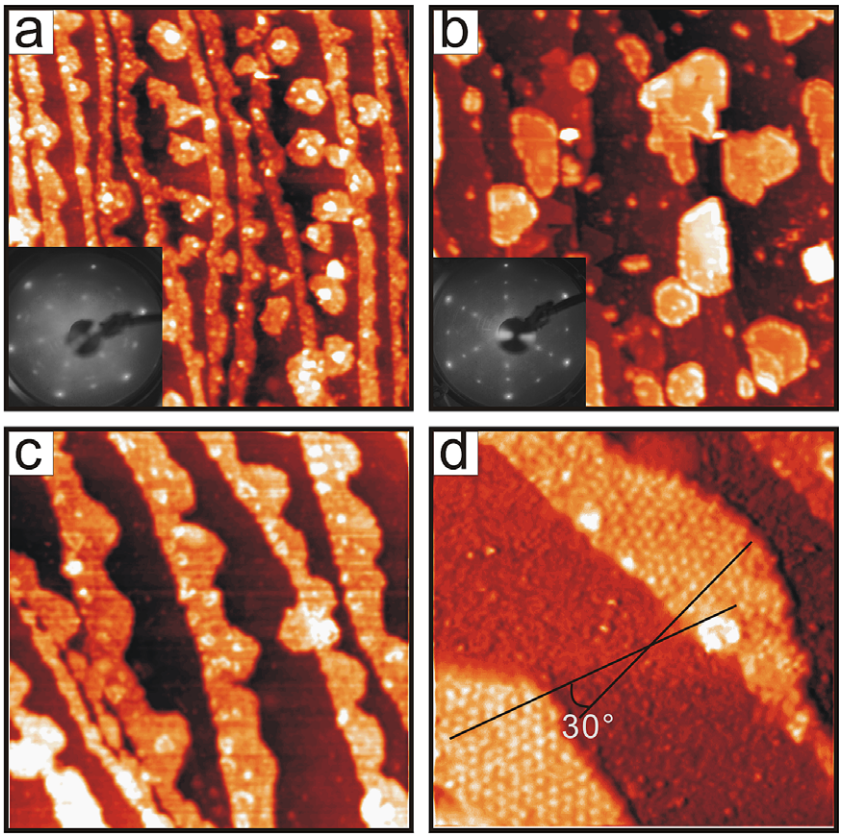


Fig. 1. STM images of 0.6 ML ceria film deposited on Ru(0 0 0 1) at 700 K (a) and 790 K (c) in $1\times10^{-7}$ mbar of $O_2$. Shown in (b) is the sample (a) further annealed in $4\times10^{-7}$ mbar $O_2$ at 900 K. The image (d) is a close up of the image (c), where two domains exhibiting the Moire structure with a ~19 Å periodicity are rotated by 30° with respect to each other. Insets in (a) and (b) show the corresponding LEED patterns. Image size is $200\times200$ nm$^2$ (a)–(c) and $60\times60$ nm$^2$ (d), tunneling parameters are: (a) $V_S = 3.3$ V, $I = 0.1$ nA; (b) $V_S = 3.6$ V, $I = 0.1$ nA; (c) $V_S = 4$ V, $I = 0.1$ nA; (d) $V_S = 3.8$ V, $I = 0.12$ nA.

aged in Fig. 1d are rotated by 30° with respect to each other, thus giving rise to the growth of rotational domains on the thicker film.

Fig. 2a and c shows $200 \times 200$ nm$^2$ STM images of thick ceria films grown at 700 K (a) and 790 K (c), respectively. The "as prepared" film at 700 K exhibits a highly corrugated surface on a long-range scale, although LEED shows sharp diffraction spots of ceria (the Ru substrate spots totally vanish at this film thickness). The 12-members ring observed in the LEED pattern shown in the inset of Fig. 2a is characteristic for hexagonal structures with two domains rotated by 30° with respect to each other. The films grown at 790 K are better ordered (see Fig. 2c), however, the terrace step edges exhibit an irregular shape, indicating limited surface diffusion at these temperatures. Deposition at even higher temperatures is accompanied by a decreasing sticking coefficient of Ce and is, therefore, not beneficial for film ordering.

As it is generally known, high temperature annealing is typically required for preparing well-ordered oxide films. When applied to ceria, the vacuum annealing above 1000 K may reduce the oxide surface or decompose the film [23,28,30]. Therefore, post-annealing of the films was performed at 980 K at higher oxygen pressure ($4 \times 10^{-7}$ mbar) than used for the ceria deposition ($1 \times 10^{-7}$ mbar). This treatment significantly improves the quality of the films as shown in Fig. 2b and d. The terraces become much broader, in particular for the films grown at 790 K (see Fig. 2d). The height of monotomic steps (~3.3 Å) and a hexagonal lattice of protrusions with a ~4 Å periodicity (see the inset in Fig. 2d) match well those for $CeO_2$(1 1 1) ($\mathbf{a}_{111} = 3.89$ Å; step height 3.1 Å). Therefore, our STM results clearly show that, for the preparation of the atomically smooth nm-thick $CeO_2$(1 1 1) films on Ru(0 0 0 1), cerium has to be deposited at elevated temperatures (~800 K) and subsequently annealed at ~1000 K, all in oxygen atmosphere (>$10^{-7}$ mbar). It is important to note, that the differences in the morphology of the films shown in Fig. 2 can hardly be discriminated by conventional LEED: all samples revealed essentially identical patterns with sharp diffraction spots of ceria.

These ceria films often show irregularly shaped depressed lines within the single terraces as shown in Fig. 3, which have been assigned to domain boundaries. The presence of the domain boundaries basically reflects a Volmer–Weber growth mode of ceria on Ru(0 0 0 1), where three-dimensional ceria islands grow independently. The formation of a first ceria monolayer wetting the metal sub-

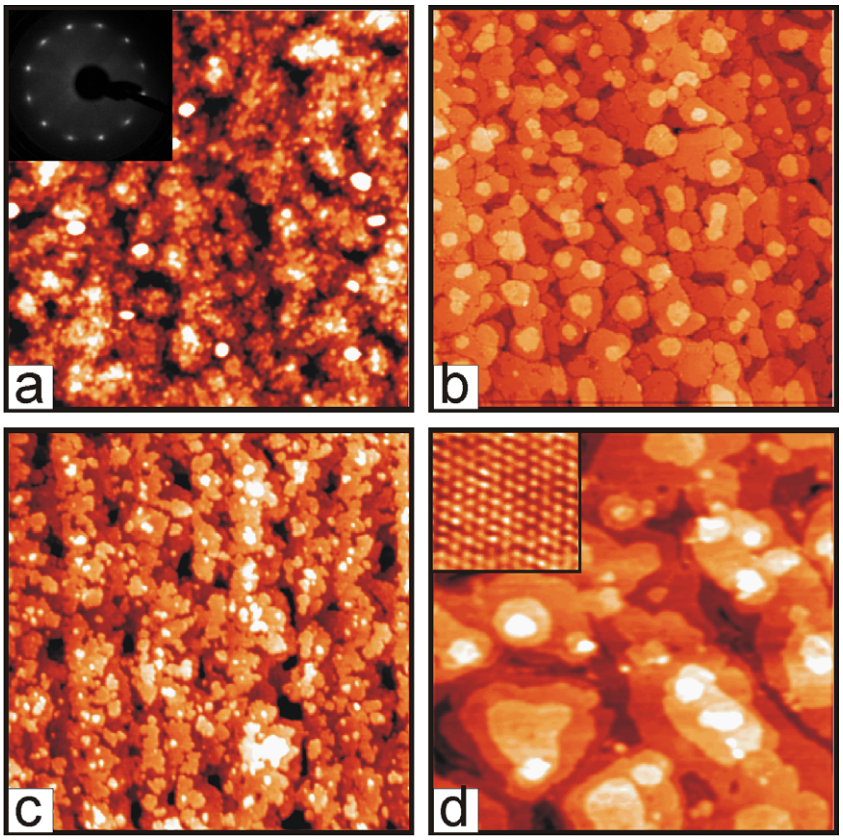


Fig. 2. (a) and (b) STM images of a 6 ML ceria film as grown at 700 K (a) and annealed at 980 K (b). (c) STM image of a 3 ML ceria film as grown at 790 K. (d) STM image of a 6 ML ceria film deposited at 790 K and annealed at 980 K. The depositions were performed in $1 \times 10^{-7}$ mbar of $O_2$ and annealing – in $4 \times 10^{-7}$ mbar of $O_2$. Inset in (a) shows a typical LEED pattern (60 eV) of the thick ceria films. Inset in (d) shows a hexagonal lattice of protrusions on the ceria surface with a ~4 Å periodicity. Size $200 \times 200$ nm$^2$ (a)–(d), $5 \times 5$ nm$^2$ (inset), tunneling parameters: (a) $V_S = 3.3$ V, $I = 0.1$ nA; (b) $V_S = 3.9$ V, $I = 0.07$ nA; (c) $V_S = 3$ V, $I = 0.1$ nA; (d) $V_S = 4$ V, $I = 0.1$ nA; (inset) $V_S = 3$ V, $I = 0.2$ nA.

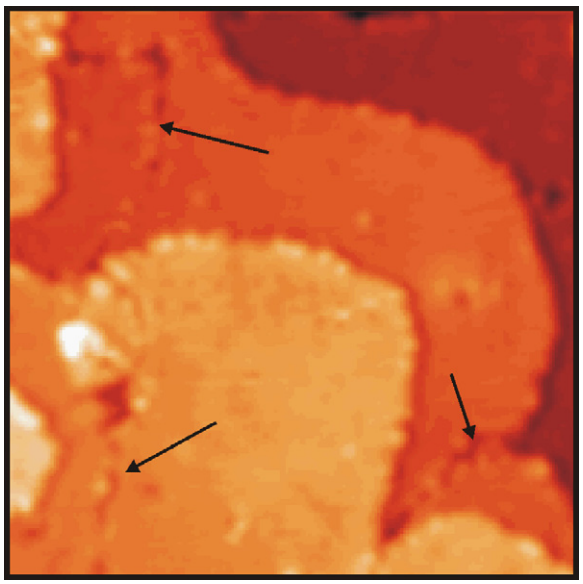

Fig. 3. STM image showing domain boundaries observed on the terraces as depressed lines, indicated by the arrows. Size $50 \times 50$ nm$^2$, $V_S = 4.2$ V, $I = 0.1$ nA.

strate, which would favor further epitaxial growth of the oxide film, seems energetically unfavorable due to the large mismatch between the oxide and the substrate. Nevertheless, increasing of the Ce deposition temperature leads to the formation of larger and better ordered ceria bi-layer islands (see Fig. 1) and, as a result, to larger terraces on the thick films (see Fig. 2).

High-resolution STM images of the ceria films have shown that the terraces exhibit a low density of point defects resolved in Fig. 4a. At the tunneling parameters applied to record this image (a bias +2.4 V to the sample, current 0.1 nA), the STM contrast originates from the states above the Fermi level, which are unoccupied Ce 4f states in nature [38–41]. Therefore, the protrusions on this image must be assigned to the Ce atoms. The protrusions seen within the depressed area (~0.2 Å below the surface), are in in-phase registry with those on the regular surface and therefore cannot be assigned to oxygen, since the O layers above and below the Ce layer in $CeO_2(1\,1\,1)$ are in out-phase registry and separated by ~1.6 Å. Tentatively, we have described the defects as three missing oxygen atoms in the top layer forming a triangle as schematically shown in Fig. 4b. Such trimer vacancies were previously observed by Nörenberg and Briggs [17] and Esch et al. [21] by imaging occupied states of oxygen. The 6 electrons left by the missing O atoms in this structure could result in the six equivalent $Ce^{3+}$ ions forming a triangle. However, independent of the oxidation state these Ce atoms are expected to appear brighter in the image since they are no longer coordinated to the topmost O atoms screening the electronic states of Ce, i.e., in contrast to the experimental observation, if no other mechanisms are involved. Note, that our STM images and the corresponding model are different from those observed and suggested for ultra-thin ceria films on Rh(1 1 1) [29], where the empty states were imaged as well, but at very different parameters (+0.5 V, 1 nA). This issue needs further investigations. For example, the defect formation may be associated with a strong relaxation of the remaining surface atoms as shown by Nolan et al. using density functional theory (DFT) [41,42]. It should be mentioned, however, that theoretical analysis of ceria surfaces is often controversial (see, for example, [40]).

Nonetheless, based on the STM images, our ceria films exhibit a low density of point defects. However, clearly visible terrace steps may contain undercoordinated Ce atoms. Assuming roughly that all these Ce atoms on the terrace perimeter are of 3+ character, we have estimated the percentage of the $Ce^{3+}$ ions on the $CeO_2(1\,1\,1)$ surface to be around 2%. Of course, this number will be by factor of 2–3 higher for the films exposing smaller terraces. There-

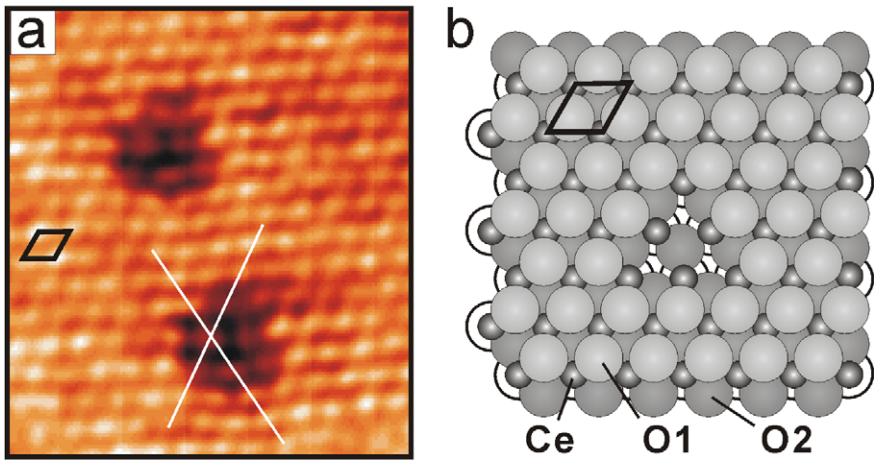


Fig. 4. STM image (a) and schematic presentation (b) of the point defects observed on the ceria films. Two crossing lines drawn over the defect show that the protrusions within the depressed areas are in in-phase registry with those on the regular surface. Only first layers of $CeO_2(1\,1\,1)$ stacked as O1–Ce–O2–O1–$\cdots$ are schematically shown. The surface unit cell is indicated. The defects imaged in (a) are assigned to the three missing O1 atoms forming a triangle. (Image size $5 \times 5$ nm$^2$, tunneling parameters: $V_S = 2.4$ V, $I = 0.16$ nA.)

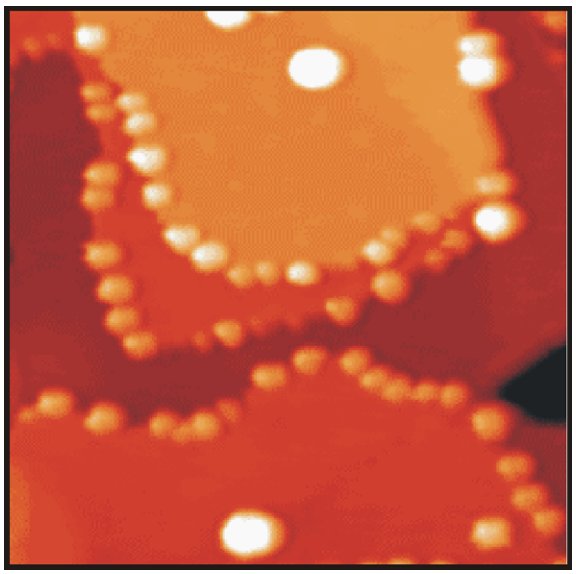

Fig. 5. STM image of 0.1 ML of Au deposited on the 6 ML ceria film at 300 K showing that majority of the Au particles nucleate on the step edges. Size $50 \times 50$ nm$^2$, $V_S = 3.8$ V, $I = 0.13$ nA.

fore, approximately 5% may be considered as an upper limit for the surface $Ce^{3+}$ concentration. In principle, this number falls into the range of values determined by photoelectron spectroscopy of the ceria films [25,28,32]. In addition, Eck et al. [28] have found that the $Ce^{3+}$:$Ce^{4+}$ ratio is strongly increased with decreasing thickness of the ceria films most likely due to small size of ceria crystallites as revealed by STM. Assuming that the noble metal particles deposited on the ceria films will nucleate on these undercoordinated sites, we have employed a "metal decoration" approach.

Fig. 5 shows a STM image of the ceria film exposed to ~0.1 ML of Au at room temperature. The image clearly demonstrates that almost all gold particles are located on the step edges. Only a few particles can be found on the terraces at this coverage, thus indicating that the films expose a low density of the point defects. (Note that this film was not exposed to LEED or AES prior to Au deposition, which may cause electron beam induced effects). It is clear that interaction of gold with the step edges is much stronger than with the O-terminated regular surface. The fact that the terraces are mostly circular suggests that the steps expose a variety of the undercoordinated atoms like edges, kinks and corners, which may act as nucleation centers for supported metal particles.

## 4. Summary

The morphology of the ceria films grown on a Ru(0001) substrate was studied by STM in combination with LEED and AES. The results show that well ordered nm-thick $CeO_2$(111) films exposing atomically flat terraces, up to 500 Å in width, can be prepared by Ce deposition in $1 \times 10^{-7}$ mbar of oxygen and post-oxidation at 980 K in $4 \times 10^{-7}$ mbar of $O_2$. The terraces exhibit a low density of point defects, assigned to oxygen vacancies, and often consist of several domains. A circular shape of terraces suggest a large variety of undercoordinated sites at the step edges which preferentially nucleate gold particles deposited onto these films. The results show that reactivity studies over ceria and metal/ceria surfaces should be complemented with STM studies, which provide direct information about the film morphology and surface defects, which are usually considered as active sites for catalysis over ceria.

## Acknowledgements

The authors gratefully acknowledge financial support by the Deutsche Forschungsgemeinschaft (DFG) through SFB 546. J.-L.L. thanks International Max-Planck Research School (IMPRS) "Complex Surfaces in Materials Science". We also thank Alexander Uhl and Martin Baron for technical assistance.

## References

[1] A. Trovarelli (Ed.), Catalysis by Ceria and Related Materials, Imperial College Press, London, 2002.
[2] S. Park, J.M. Vohs, R.J. Gorte, Nature 404 (2000) 265.
[3] G.A. Deluga, J.R. Salge, L.D. Schmidt, X.E. Verykios, Science 303 (2004) 993.
[4] O. Dolub, W. Hebenstreit, U. Diebold, Phys. Rev. Lett. 84 (2000) 3646.
[5] R.A. Bennett, P. Stone, M. Bowker, Catal. Lett. 59 (1999) 994.
[6] T. Schalow, M. Laurin, B. Brandt, S. Schauermann, S. Guimond, H. Kuhlenbeck, D.E. Starr, S.K. Shaikhutdinov, J. Libuda, H.-J. Freund, Angew. Chem. Int. Ed. 44 (2005) 7610.
[7] Q. Fu, H. Saltsburg, M. Flytzani-Stephanopoulos, Science 301 (2003) 935.
[8] U.R. Pillai, S. Deevi, Appl. Catal. A 299 (2005) 266.
[9] J. Guzman, S. Carrettin, A. Corma, J. Am. Chem. Soc. 127 (2005) 3286.
[10] S. Carrettin, P. Concepción, A. Corma, J.M. López Nieto, V.F. Puntes, Angew. Chem. Int. Ed. 43 (2004) 2538.
[11] R. Meyer, C. Lemire, S. Shaikhutdinov, H.-J. Freund, Gold Bull. 37 (2004) 72.
[12] D.T. Thompson, Appl. Catal. A 243 (2003) 201.
[13] M. Sterrer, M. Yulikov, E. Fischbach, M. Heyde, H.-P. Rust, G. Pacchioni, T. Risse, H.-J. Freund, Angew. Chem. Int. Ed. 45 (2006) 2630.
[14] B. Yoon, H. Häkkinen, U. Landman, A.S. Wörz, J.-M. Antonietti, S. Abbeit, K. Judai, U. Heiz, Science 307 (2005) 403.
[15] A. Del Vitto, G. Pacchioni, F. Delbecq, P. Sautet, J. Phys. Chem. B 109 (2005) 8040.
[16] L. Giordano, J. Goniakowski, G. Pacchioni, Phys. Rev. B 64 (2001) 075417.
[17] H. Nörenberg, G.A.D. Briggs, Phys. Rev. Lett. 79 (1997) 4222.
[18] H. Nörenberg, G.A.D. Briggs, Surf. Sci. 424 (1999) L352.
[19] H. Nörenberg, J.H. Harding, Surf. Sci. 477 (2001) 17.
[20] Y. Namai, K.-I. Fukui, Y. Iwasawa, Catal. Today 85 (2003) 79.
[21] F. Esch, S. Fabris, L. Zhou, T. Montini, C. Africh, P. Fornasiero, G. Comelli, R. Rosei, Science 309 (2005) 752.
[22] J.M. Vohs, T. Feng, G.S. Wong, Catal. Today 85 (2003) 303.
[23] M. Alexandrou, R.M. Nix, Surf. Sci. 321 (1994) 47.
[24] C. Hardacre, G.M. Roe, R.M. Lambert, Surf. Sci. 326 (1995) 1.
[25] K.-D. Schierbaum, Surf. Sci. 399 (1998) 29.
[26] U. Berner, K. Schierbaum, Phys. Rev. B 65 (2002) 235404.

[27] U. Berner, K. Schierbaum, G. Johnes, P. Wincott, S. Haq, G. Thornton, Surf. Sci. 467 (2000) 201.
[28] S. Eck, C. Castellarin-Cudia, S. Surnev, M.G. Ramsey, F.P. Netzer, Surf. Sci. 520 (2002) 173.
[29] C. Castellarin-Cudia, S. Surnev, G. Schneider, R. Podlucky, M.G. Ramsey, F.P. Netzer, Surf. Sci. 554 (2004) L120.
[30] A. Siokou, R.M. Nix, J. Phys. Chem. B 103 (1999) 6984.
[31] W. Xiao, Q. Guo, E.G. Wang, Chem. Phys. Lett. 368 (2003) 527.
[32] D.R. Mullins, P.V. Radulovic, S.H. Overbury, Surf. Sci. 429 (1999) 186.
[33] D.R. Mullins, L. Kundakovic, S.H. Overbury, J. Catal. 195 (2000) 169.
[34] S.H. Overbury, D.R. Mullins, D.R. Huntley, L. Kundakovic, J. Catal. 186 (1999) 296.
[35] D.R. Mullins, M.D. Robbins, J. Zhou, Surf. Sci. 600 (2006) 1547.
[36] E.L. Wilson, W.A. Brown, G. Thornton, Surf. Sci. 600 (2006) 2555.
[37] J. Yang, X. Wang, C. Jiang, H. Xiao, L. Lu, Surf. Interf. Anal. 38 (2006) 498.
[38] N.V. Skorodumova, M. Baudin, K. Hermansson, Phys. Rev. B 69 (2004) 075401.
[39] S. Fabris, S. Gironcoli, S. Baroni, G. Vicario, G. Balducci, Phys. Rev. B 71 (2005) 041102.
[40] S. Fabris, S. Gironcoli, S. Baroni, G. Vicario, G. Balducci, Phys. Rev. B 72 (2005) 237102.
[41] M. Nolan, S. Grigoleit, D.C. Sayle, S.C. Parker, G.W. Watson, Surf. Sci. 576 (2005) 217.
[42] M. Nolan, S.C. Parker, G.W. Watson, Surf. Sci. 595 (2005) 223.